ChemPubSoc Europe

DOI: 10.1002/open.201800001

Open Access ChemistryOPEN Communications

Hierarchical SAPO-34 Architectures with Tailored Acid Sites using Sustainable Sugar Templates

Ivana Miletto,[a] Chiara Ivaldi,[a] Geo Paul,[a] Stephanie Chapman,[b] Leonardo Marchese,[a] Robert Raja,[b] and Enrica Gianotti*[a]

In a distinct, bottom-up synthetic methodology, monosaccharides (fructose and glucose) and disaccharides (sucrose) have been used as mesoporogens to template hierarchical SAPO-34 catalysts. Detailed materials characterization, which includes solid-state magic angle spinning NMR and probe-based FTIR, reveals that, although the mesopore dimensions are modified by the identity of the sugar template, the desirable acid characteristics of the microporous framework are retained. When the activity of the hierarchical SAPO-34 catalysts was evaluated in the industrially relevant Beckmann rearrangement, under liquid-phase conditions, the enhanced mass-transport properties of sucrose-templated hierarchical SAPO-34 were found to deliver a superior yield of ε-caprolactam.

Zeotype materials are a prominent and well-established class of industrial heterogeneous catalysts, particularly for acid-catalyzed chemical transformations.

Silicoaluminophosphates (SAPOs) have been widely employed as solid-acid catalysts;[1,2] most notable is SAPO-34 with a chabazite (CHA) topological structure, which is the industrial methanol-to-olefin (MTO) catalyst (100% methanol conversion and >90% selectivity to C_2–C_4 light olefins).[3,5] However, the narrow pore aperture (3.8×3.8 Å) of microporous SAPO-34 severely impedes molecular motion, which expedites pore blockage owing to coke deposition with prolonged time-on-stream.[6] To address rapid degradation of the catalytic performance that can encumber SAPO-34 (and other microporous materials) hierarchical analogues are being developed. These hierarchical systems typically retain the microporous structure in the bulk, but possess an additional mesoporous network that improves mass transport to the internal active sites. Hierarchical SAPO-34 has been synthesized using both top-down[7–9] and bottom-up[10–12] approaches. In a top-down synthesis, a post-synthetic treatment, such as demetallation, is used to generate mesoporous cavities, although this is accompanied by the production of defect sites that modify the textural and acid properties of the catalyst. The alternative bottom-up approach ensures a high degree of structural control of the SAPOs, with retention of the active sites associated with the microporous analogue.[12] Typically, bottom-up preparations use a sophisticated surfactant soft-template (such as an organosilane) that is added to the synthesis gel to template mesoporosity.[11,13] However, in a recent drive towards low-cost, sustainable mesoporogens, saccharides have been identified as viable candidates for mesopore formation.[14] Owing to the immense catalytic potential of hierarchically porous materials, the development of new and effective strategies for synthesizing materials with dual porosity is timely. Ideally, such procedures would be able to yield a hierarchical framework by means of a simple, low-cost template, and would be compatible with the conventional, one-pot synthesis. In this Communication, we report a novel and distinct bottom-up approach for the synthesis of hierarchical SAPO-34, which mitigates the need for sophisticated surfactants, by employing monosaccharides (glucose or fructose) or disaccharides (sucrose) as the mesopore-directing agent.[15,16]

Hierarchical SAPO-34 catalysts were synthesized from a gel of molar composition 1.0 Al / 1.0 P / 0.6 Si / 0.067 SDA_{meso} / 1 TEAOH / 60 H_2O under hydrothermal conditions at 200 °C for 72 h, using tetraethylammonium hydroxide (TEAOH) as the structure-directing agent (SDA) for the micropores, and glucose, fructose or sucrose as the mesoporogen (SDA_{meso}). For comparison, microporous SAPO-34 was prepared under identical conditions, excluding the addition of a saccharide mesoporogen. All catalysts were calcined in air flow at 873 K for 16 h to remove the organic templates.

In Table 1, inductively coupled plasma (ICP) chemical analyses are reported for the catalysts employed in this study. Importantly, the Si/(Si + Al + P) ratio for hierarchical SAPO-34, as determined by ICP analysis, is in good agreement with the synthesis gel composition.

SEM reveals that the hierarchical SAPO-34 catalysts exhibit spherical aggregates of nano-sized rhombohedra (Figure S1), with a relatively homogeneous distribution of size and shape, with some (minimal) hexagonal crystals. The particles of these saccharide-templated materials are also generally larger than those of the microporous SAPO-34 (Figures S1 L and S1 M), with the latter comprising particles of rhombohedral shape

[a] Dr. I. Miletto, C. Ivaldi, Dr. G. Paul, Prof. L. Marchese, Prof. E. Gianotti
Department of Science and Technological Innovation
Università del Piemonte Orientale
Viale T. Michel 11, 15121 Alessandria (Italy)
E-mail: enrica.gianotti@uniupo.it

[b] S. Chapman, Prof. R. Raja
School of Chemistry
Faculty of Natural and Environmental Sciences
University of Southampton
SO17 1BJ Southampton (UK)

Supporting Information and the ORCID identification number(s) for the author(s) of this article can be found under https://doi.org/10.1002/open.201800001.

Table 1. ICP chemical analysis of SAPO-34 catalysts.

Acronym	SDA_{meso}	Si [wt%]	Al [wt%]	P [wt%]	Si/ Si + Al + P[a]	Si/ Si + Al + P[b]
GLU-S01	glucose	8.08	15.05	12.64	0.23	0.23
FRU-S02	fructose	6.93	15.79	13.05	0.19	0.23
SUC-S03	sucrose	8.22	20.50	14.10	0.19	0.23

[a] Experimental framework composition determined by ICP analysis after the synthesis. [b] Theoretical framework composition determined from the synthesis gel composition.

morphology, as is typical of CHA crystals. Energy-dispersive X-ray (EDX) spectroscopic analyses (Figures S1 C, S1 F, S1 I, and S1 N) collected in different regions of the SAPO-34 samples reveal a homogeneous distribution of Al, P, and Si. By comparing the XRD spectra of the calcined hierarchical catalysts (Figure 1 A) with that of microporous SAPO-34, all observable peaks were attributed to the CHA framework, excluding the presence of any secondary phase.[17]

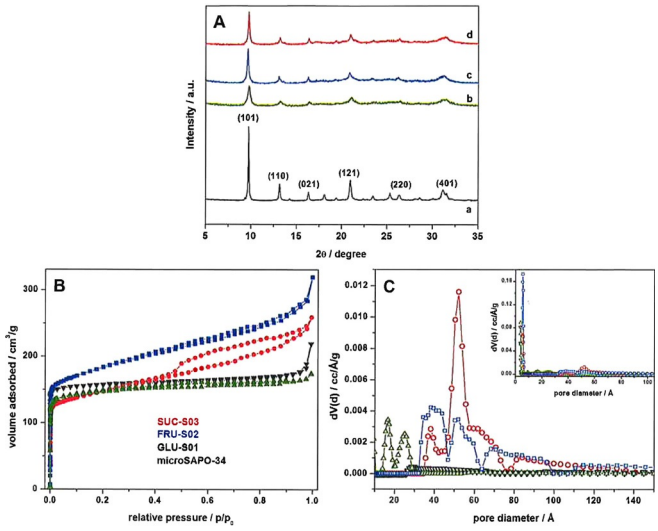

Figure 1. A) The powder XRD pattern of microporous SAPO-34 (a), GLU-S01 (b), FRU-S02 (c), and SUC-S03 (d). B) The N_2 adsorption/desorption isotherms at 77 K. C) The pore-size distribution in the mesopore range, with pore-size distribution in the micropore and mesopore range (inset).

The textural properties of hierarchical SAPO-34 were assessed by N_2 adsorption/desorption volumetric analysis at 77 K (Figures 1 B and 1 C).[18] Although microporous SAPO-34 and GLU-S01 reveals the Type I isotherm that is typical of a microporous framework, enhanced N_2 uptake at intermediate-to-high pressures is observed for both SUC-S03 and FRU-S02 samples, yielding the Type IV isotherm characteristic of a mesoporous material (Figures 1 B and S2). The pore-size distribution of microporous SAPO-34, obtained by using non-localized density functional theory (NLDFT) method, was found to be consistent with the microporous CHA structure (Figure 1 C, inset), whereas FRU-S02 and SUC-S03 exhibit mesopores of approximately 38 and 52 Å (Figure 1 C). Beside the micropores of the CHA structure, GLU-S01 also affords small mesopores of 17 and 25 Å diameter. With respect to microporous SAPO-34, both SUC-S03 and FRU-S02 exhibit substantial enhancements in mesopore volume (V_{meso}), total pore volume (V_{tot}), and mesopore surface area (S_{meso}) (Table S1). Conversely, GLU-S01 presents a low mesopore surface area and pore volume, being more akin to microporous SAPO-34. Volumetric data strongly support the successful preparation of hierarchical SAPO-34 when fructose or sucrose are used as the mesoporogen, where there is evidence for the coexistence of multiple levels of porosity.

Thermogravimetric and derivative thermogravimetric analyses (TGA/DTG) of the hierarchical SAPO-34 systems (Figures S3 and S4) exhibit peaks at 430 °C, which can be attributed to the removal of organic template species (TEAOH and saccharides). In contrast, the decomposition of TEAOH (the micropore SDA) within microporous SAPO-34 is identified by a peak at approximately 250 °C. As such, we propose interconnectivity of the micro- and mesopores in the hierarchical systems, such that the micropore SDA cannot be eliminated until the sugar template has been decomposed at higher temperature.

The catalytic potential of the hierarchical SAPO-34 catalysts was evaluated in the liquid-phase Beckmann rearrangement of cyclohexanone oxime to ε-caprolactam (the precursor to the Nylon-6 polymer) and compared with that of microporous SAPO-34 (Figure 2). Conventional microporous SAPO-34 is characterized by poor activity in the liquid-phase Beckmann rearrangement, owing to the inaccessibility of the internal active sites to cyclohexanone oxime. As a result, only around 15% yield is achieved after 6 h of reaction. Notably, the glucose-templated catalyst shows comparable (or even lower) activity, which can likely be attributed to the lower surface area available for active site interactions. SUC-S03 shows the best activity among the hierarchical catalysts, achieving over 40% yield in the same 6 h period. Interestingly, the performance of FRU-S02 is noticeably inferior to that of SUC-S03. The activity of the SUC-S03 is noteworthy, given that the Beckmann rearrangement is conventionally performed at temperatures above 325 °C (vapor phase), and a three-fold increase in catalytic activity (when compared with its microporous analogue) highlights the superior diffusion afforded by the hierarchical archi-

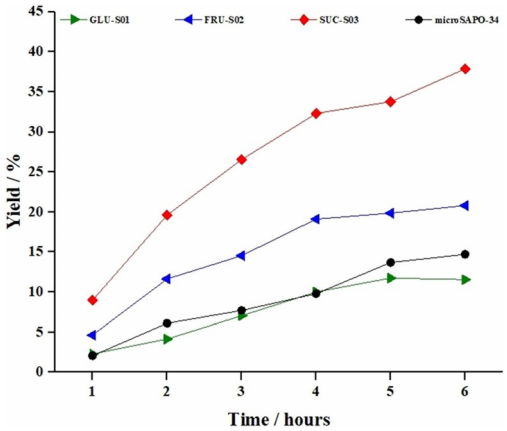

Figure 2. A comparison of the yield of ε-caprolactam in the liquid-phase Beckmann rearrangement at 130 °C, benzonitrile solvent.

tecture at lower temperatures (130 °C). To understand the diverse behavior of the hierarchical SAPO-34 catalysts and to assess the nature, strength, and accessibility of the acid sites, spectroscopic characterization using solid-state magic angle spinning NMR (SS MAS NMR) and probe FTIR was performed.

The chemical environment of the framework atoms in hierarchical and microporous SAPO-34 was evaluated by ^{27}Al, ^{31}P, and ^{29}Si MAS NMR (Figure S5). The ^{27}Al and ^{31}P spectra of microporous and hierarchical SAPO-34 evidenced the presence of tetrahedrally coordinated Al (signal at ca. 36 ppm, Figure S4 A) and P atoms (signal at −29.8 ppm, Figure S4 B), confirming strict alternation of Al and P at the T positions of the AlPO framework.[19] The ^{31}P spectra of hierarchical materials also present a tail at approximately −24 ppm, owing to P–OH defects.[12] The ^{29}Si NMR spectra of microporous SAPO-34 exhibits signals at −92, −96, and −101 ppm, owing to tetrahedral framework Si coordinated to four, three, and two Al atoms (Figure S4 C). Hierarchical materials showed the same three resonances as a composite of narrow and broad signals at the same positions; an additional signal is also present for Q_4 silicon sites (−110 ppm), which revealed the formation of Si islands.

The nature of the acid sites in hierarchical SAPO-34 was investigated by using ^{1}H SS MAS NMR and FTIR spectroscopies (Figure S6). ^{1}H SS NMR reveals different proton environments in the SAPO-34 materials (Figure 3). A signal at around 4 ppm, associated with Brønsted Si(OH)Al groups, is observed in both microporous and hierarchical SAPO-34 catalyst.

After deconvolution, two components (at 3.6 and 4 ppm) can be differentiated and attributed to two types of Brønsted acid sites in the O4 and O2 structural configuration of the CHA framework.[20] Moreover, quantitative analysis by ^{1}H MAS NMR indicates that the number of Brønsted acid sites is comparable in all hierarchical SAPO-34 systems (Table 2). Weak signals at 2.6 ppm (attributed to P–OH species) and 1.8 ppm (attributed to Si–OH species) are also present in hierarchical materials, whereas proton resonances beyond 4.5 ppm are attributed to hydrogen-bonded species.[12,21]

The accessibility and strength of the acid sites in hierarchical SAPO-34 were assessed by FTIR spectroscopy of adsorbed basic probe molecules. Firstly, to quantify the total amount of Brønsted acid sites, NH_3 (0.26 nm kinetic diameter) was used. Owing to its small diameter, NH_3 can enter both the mesopores and micropores of hierarchical SAPO-34 framework and thus interact with Brønsted sites that are inaccessible to larger molecules, such as substituted pyridines.

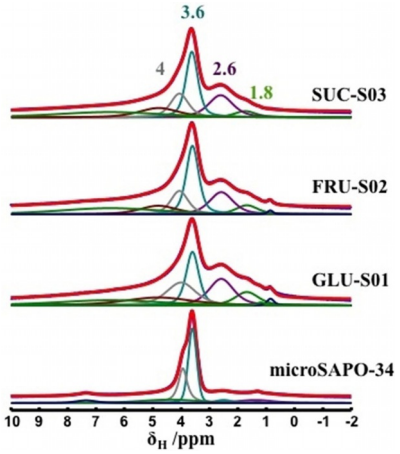

Figure 3. ^{1}H MAS NMR spectra of calcined microporous SAPO-34 and hierarchical GLU-S01, FRU-S02, and SUC-S03.

For this reason, 2,4,6-trimethylpyridine (2,4,6-TMP) is widely used to study the enhanced accessibility of acid sites in hierarchical zeolites, exploiting the impeded diffusion through small micropores.[21–23] By contrasting the interactions of NH_3 and 2,4,6-TMP probes, it is possible to extract information relating to the accessibility of the Brønsted acid sites.[12,21]

Upon NH_3 adsorption (Figure 4 A–C), the bending mode of ammonia H-bonded to Si–OH or P–OH is detected at 1619 cm^{-1}. Furthermore, the band at 1450 cm^{-1}, owing to the δ_{as} of the NH_4^+ ions, indicates NH_3 protonation by Brønsted acid sites. 2,4,6-TMP (kinetic diameter ca. 0.74 nm) is too bulky to enter the micropores of SAPO-34, but will interact with acid sites located within the mesopores or at the micropore mouths of hierarchical SAPO-34. When 2,4,6-TMP interacts with a Brønsted acid site, its inherent basicity ($pK_a = 7.59$) induces proton transfer, yielding the protonated 2,4,6-TMPH$^+$ species. The ν_{8a} C–C stretching mode of 2,4,6-TMP (which has a liquid-phase frequency of 1611 cm^{-1}) is very sensitive to the Brønsted sites in the hierarchical materials, with its position changing in response to acid-site strength. When the ν_{8a} mode appears at wavenumbers >1630 cm^{-1}, the formation of the protonated species (2,4,6-TMPH$^+$) is inferred, whereas a lower wavenumber indicates the formation of a H-bonded adduct or physisorbed species.[12,21] Upon 2,4,6-TMP adsorption on FRU-S02 and SUC-S03 (Figures 4 D and 4 E), bands at 1611 and 1575 cm^{-1} (owing to physisorbed 2,4,6-TMP) and a signal at 1638 cm^{-1} (owing to 2,4,6-TMPH$^+$) are observed. The physisorbed molecules are readily removed upon outgassing at 298 K, but the

Table 2. Distribution of protonic species obtained from single pulse ^{1}H MAS NMR spectroscopy in microporous and hierarchical SAPO-34. FTIR frequencies of the corresponding OH groups are also reported.

ν_{OH} [cm^{-1}]	^{1}H chemical shift (δ) [ppm]	Assignment	^{1}H species [%] GLU-S01	FRU-S02	SUC-S03	microSAPO-34
3745	1.8	Si–OH	9	7	5	–
3678	2.6	P–OH	19	18	20	4
3630	3.6	Brønsted acid sites	21	30	29	42
3600	4.0	Brønsted acid sites	20	14	16	27
3550–3350	5.5 (centered)	H-bonded species	29	30	30	18

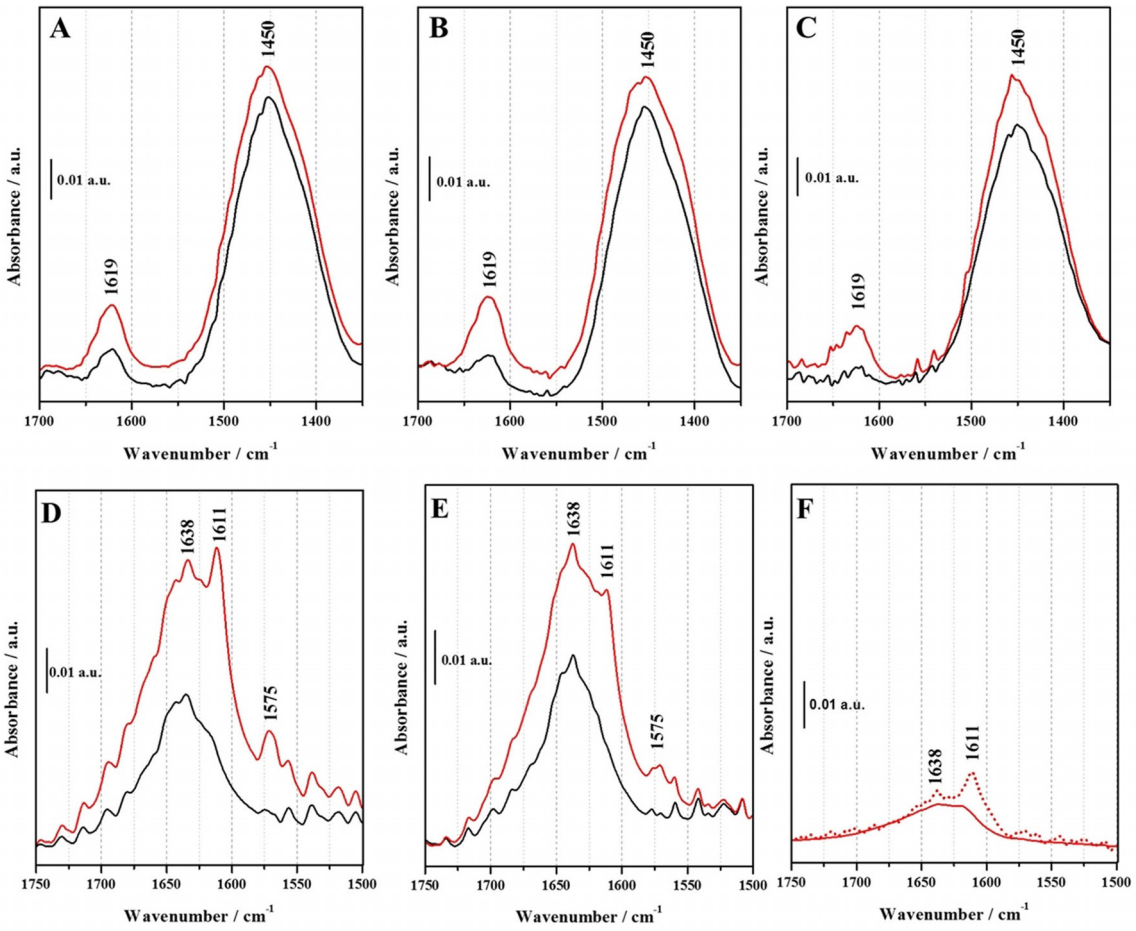

Figure 4. FTIR difference spectra of NH_3 adsorption (90 mbar) on GLU-S01 (A), FRU-S02 (B), and SUC-S03 (C) and of 2,4,6-TMP adsorption (vapor pressure) on FRU-S02 (D), SUC-S03 (E), and GLU-S01 and microporous SAPO-34 (F, solid and dotted line, respectively). The spectra are shown before (red curve) and after outgassing the probe molecules at 298 K (black curve).

retention of the 1638 cm^{-1} band indicates that a fraction of Brønsted acid sites are made accessible by the mesoporous network. The protonated species are not observed on microporous SAPO-34 or GLU-S01 (Figure 4F), indicating that, in the latter case, the mesopores detected by volumetric analysis are irrelevant to accessibility arguments. The total number of accessible Brønsted acid sites (*N*) of hierarchical SAPO-34 materials determined by using NH_3 and 2,4,6-TMP is reported in Table 3, together with the nature and the IR position of the bands of their protonated species. The total number of Brønsted acid sites (*N*) determined by ammonia adsorption was found to be comparable for all hierarchical catalysts (Table 3). The accessibility factor (AF) is similar for FRU-S02 and SUC-S03, although only a small fraction of the total Brønsted acid sites are accessible to the bulky 2,4,6-TMP probe.

Physicochemical characterization and catalytic data have highlighted that saccharide templating with fructose and sucrose is an effective means of preparing hierarchical SAPO-34, thus introducing secondary porosity without the need for a sophisticated mesoporogen. In contrast, the glucose template has been proven to be essentially ineffective at introducing mesoporosity, yielding a catalyst with textural properties inferior to microporous SAPO-34. The inefficacy of glucose as a mesoporogen may be attributed to the low concentration used in the synthesis gel. Nandan et al.[14] reported that a low glucose concentration produces smaller mesopores and textural features similar to microporous analogues.

Table 3. The concentration of accessible Brønsted acid sites (*N*) in hierarchical SAPO-34

	Protonated species	Position of IR band of protonated species [cm^{-1}]	*N* [mmol g^{-1}]	AF
GLU-S01	NH_4^+ [a]	1450 (δ_{as})	43.88	1
FRU-S02	NH_4^+ [a]	1450 (δ_{as})	40.39	1
	2,4,6-$TMPH^+$ [b]	1638 (ν_{8a})	3.13	0.077
SUC-S03	NH_4^+ [a]	1450 (δ_{as})	40.73	1
	2,4,6-$TMPH^+$ [b]	1638 (ν_{8a})	2.95	0.072

[a] $\varepsilon = 0.147$ cm^2 μmol^{-1}.[24] [b] $\varepsilon = 0.62$ cm^2 μmol^{-1}.[23]

The acid properties of the hierarchical SAPO-34 were found to be comparable to the microporous analogue, although a fraction of Brønsted acid sites were more accessible when fructose or sucrose was used as the template. Thus, by using this approach, it is possible to achieve effective modulation of mesopore dimensions by selecting an appropriate (mono- or di-) saccharide mesoporogen, without modifying the acid proper-

ties. It is the enhanced mass-transport capabilities, which were maximized when sucrose was used as templating agent, that were found to be influential in enhancing the catalytic performance of hierarchical SAPO-34 in the liquid-phase Beckmann rearrangement.

Experimental Section

Hierarchical SAPO-34 Synthesis

Aluminum isopropoxide (7.00 g, Sigma Aldrich) was added slowly to phosphoric acid (2.35 mL, 85% in H_2O, Sigma Aldrich) previously diluted in deionized water (29 mL), and the mixture was stirred for 1 h. Fumed silica (1.24 g, Sigma Aldrich) was slowly added and the mixture was further stirred for 2 h. TEAOH (14.00 mL, 35 wt% in H_2O, Sigma Aldrich) was added dropwise while stirring, and the gel was further stirred for 4 h. The saccharide template (SDA_{meso}), preventively dissolved in deionized water (8 mL), was added and the resulting gel (with the molar composition 1.0 Al / 1.0 P / 0.6 Si / 0.067 SDA_{meso} / 1 TEAOH / 60 H_2O) was vigorously stirred for 30 min . The gel was transferred to a Teflon-lined stainless-steel autoclave and crystallized at 453 K for 72 h under autogenous pressure. The solid product was then recovered by filtration and washed with water. The as-prepared product was dried in air at 373 K and calcined in a tube furnace under air flow at 873 K for 16 h to produce a white crystalline solid.

Acknowledgements

The project leading to these results has received funding from the European Union's Horizon 2020 research and innovation program under grant agreement N. 720783—MULTI2HYCAT. S.C. thanks Advansix for a PhD scholarship.

Conflict of Interest

The authors declare no conflict of interest.

Keywords: acid catalysis · bottom-up synthesis · hierarchical SAPO-34 · physicochemical characterization · sustainable templates

[1] M. Hartmann, L. Kevan, *Chem. Rev.* **1999**, *99*, 635 – 664.
[2] E. Gianotti, M. Manzoli, M. E. Potter, V. N. Shetti, D. Sun, J. Paterson, T. M. Mezza, A. Levy, R. Raja, *Chem. Sci.* **2014**, *5*, 1810 – 1819.
[3] B. Vora, J. Q. Chen, A. Bozzano, B. Glover, P. Barger, *Catal. Today* **2009**, *141*, 77 – 83.
[4] D. Chen, K. Moljordand, A. Holmen, *Microporous Mesoporous Mater.* **2012**, *164*, 239 – 250.
[5] P. Tian, Y. Wei, M. Ye, Z. Liu, *ACS Catal.* **2015**, *5*, 1922 – 1938.
[6] X. Zhu, J. P. Hofmann, B. Mezari, N. Kosinov, L. Wu, Q. Qian, B. M. Weckhuysen, S. Asahina, J. Ruiz-Martinez, E. J. M. Hensen, *ACS Catal.* **2016**, *6*, 2163 – 2177.
[7] D. Verboekend, M. Milina, J. Perez-Ramirez, *Chem. Mater.* **2014**, *26*, 4552 – 4562.
[8] X. Chen, A. Vicente, Z. Qin, V. Ruaux, J. P. Gilson, V. Valtchev, *Chem. Commun.* **2016**, *52*, 3512 – 3515.
[9] D. Xi, Q. Sun, X. Chen, N. Wang, Y. Yu, *Chem. Commun.* **2015**, *51*, 11987 – 11989.
[10] C. Wang, M. Yang, P. Tian, S. Xu, Y. Yang, D. Wang, Y. Yuan, Z. Liu, *J. Mater. Chem. A* **2015**, *3*, 5608 – 5616.
[11] S. H. Newland, W. Sinkler, T. Mezza, S. R. Bare, M. Caravetta, I. M. Haies, A. Levy, S. Keenan, R. Raja, *ACS Catal.* **2015**, *5*, 6587 – 6593.
[12] I. Miletto, G. Paul, S. Chapman, G. Gatti, L. Marchese, R. Raja, E. Gianotti, *Chem. Eur. J.* **2017**, *23*, 9952 – 9961.
[13] Q. Sun, N. Wang, D. Xi, M. Yang, J. Yu, *Chem. Commun.* **2014**, *50*, 6502 – 6505.
[14] D. Nandan, S. K. Saxena, N. Viswanadham, *J. Mater. Chem. A* **2014**, *2*, 1054 – 1059.
[15] X. Yang, T. Lu, C. Chen, L. Zhou, F. Wang, Y. Su, J. Xu, *Microporous Mesoporous Mater.* **2011**, *144*, 176 – 182.
[16] Z. Liu, L. Liu, H. Song, C. Wang, W. Xing, S. Komarneni, Z. Yan, *Mater. Lett.* **2015**, *154*, 116 – 119.
[17] A. M. Prakash, S. Unnikrishnan, *J. Chem. Soc. Faraday Trans.* **1994**, *90*, 2291 – 2296.
[18] K. A. Cychosz, R. Guillet-Nicolas, J. Garcia-Martinez, M. Thommes, *Chem. Soc. Rev.* **2017**, *46*, 389 – 414.
[19] B. Zibrowius, E. Loffler, M. Hunger, *Zeolites* **1992**, *12*, 167 – 174.
[20] a) G. A. V. Martins, G. Berlier, S. Coluccia, H. O. Pastore, G. B. Superti, G. Gatti, L. Marchese, *J. Phys. Chem. C* **2007**, *111*, 330 – 339; b) G. V. A. Martins, G. Berlier, C. Bisio, S. Coluccia, H. O. Pastore, L. Marchese, *J. Phys. Chem. C* **2008**, *112*, 7193 – 7200.
[21] A. Erigoni, S. H. Newland, G. Paul, L. Marchese, R. Raja, E. Gianotti, *ChemCatChem* **2016**, *8*, 3161 – 3169.
[22] F. Thibault-Starzyk, I. Stan, S. Abellu, A. Bonilla, K. Thomas, C. Fernandez, J.-P. Gilson, J. Perez-Ramirez, *J. Catal.* **2009**, *264*, 11 – 14.
[23] K. Mlekodaj, K. Tarach, J. Datka, K. Gura-Marek, W. Makowski, *Microporous Mesoporous Mater.* **2014**, *183*, 54 – 61.
[24] J. Datka, B. Gil, A. Kubacka, *Zeolites* **1995**, *15*, 501 – 506.

Received: January 2, 2018
Revised manuscript received: January 26, 2018

